arXiv:2201.05699v1 [cond-mat.mtrl-sci] 14 Jan 2022

Transport and optical properties of the chiral semiconductor Ag_3AuSe_2

Juyeon Won,[1] Soyeun Kim,[2,3] Martin Gutierrez-Amigo,[4,5] Simon Bettler,[2,3] Bumjoo Lee,[6,7] Jaeseok Son,[6,7] Tae Won Noh,[6,7] Ion Errea,[8,5,9] Maia G. Vergniory,[8,10] Peter Abbamonte,[2,3] Fahad Mahmood,[2,3] and Daniel P. Shoemaker[1,*]

[1]*Department of Materials Science and Engineering and Materials Research Laboratory, University of Illinois at Urbana-Champaign, Urbana, IL 61801, USA*
[2]*Department of Physics, University of Illinois at Urbana-Champaign, Urbana, 61801 IL, USA*
[3]*Materials Research Laboratory, University of Illinois at Urbana-Champaign, Urbana, 61801 IL, USA*
[4]*Department of Physics, University of the Basque Country (UPV/EHU), Apartado 644, 48080 Bilbao, Spain*
[5]*Centro de F'isica de Materiales (CSIC-UPV/EHU), Manuel de Lardizabal Pasealekua 5, 20018 Donostia/San Sebastián, Spain*
[6]*Center for Correlated Electron Systems, Institute for Basic Science, Seoul 08826, Republic of Korea*
[7]*Department of Physics and Astronomy, Seoul National University, Seoul 08826, Republic of Korea*
[8]*Donostia International Physics Center, P. Manuel de Lardizabal 4, 20018 Donostia-San Sebastian, Spain*
[9]*Fisika Aplikatua 1 Saila, Gipuzkoako Ingeniaritza Eskola, University of the Basque Country (UPV/EHU), Europa Plaza 1, 20018 Donostia/San Sebastián, Spain*
[10]*Max Planck Institute for Chemical Physics of Solids , 01187 Dresden, Germany*

Previous band structure calculations predicted Ag_3AuSe_2 to be a semiconductor with a band gap of approximately 1 eV. Here, we report single crystal growth of Ag_3AuSe_2 and its transport and optical properties. Single crystals of Ag_3AuSe_2 were synthesized by slow-cooling from the melt, and grain sizes were confirmed to be greater than 2 mm using electron backscatter diffraction. Optical and transport measurements reveal that Ag_3AuSe_2 is a highly resistive semiconductor with a band gap of and activation energy around 0.3 eV. Our first-principles calculations show that the experimentally-determined band gap lies between the predicted band gaps from GGA and hybrid functionals. We predict band inversion to be possible by applying tensile strain. The sensitivity of the gap to Ag/Au ordering, chemical substitution, and heat treatment merit further investigation.

I. INTRODUCTION

Ag_3AuSe_2 was first reported reported in 1971 as the mineral fischesserite from Předbořice, Czech Republic, by Johan, et al.[1] It was the first gold-containing selenide reported, and its crystal structure was identified as isostructural to the chiral mineral petzite Ag_3AuTe_2 in space group $I4_132$. Moderate reflectivity in the visible range and a Moh's hardness of two were corroborated on another natural sample in 2004.[2] Initial work on the silver-gold chalcogenides used differential thermal analysis (DTA) to show that they undergo order-disorder transitions to body-centered cubic Ag_2S phases upon heating, with Ag_3AuSe_2 transforming at 270°C.[3] The tellurite Ag_3AuTe_2 undergoes two transitions at 220°C and 320°C, with the intermediate crystal structure unknown, even though high-temperature X-ray diffraction (XRD) data were collected.[4] The sulfide uytenbogaardtite, on the other hand, has a more complex distorted tetragonal $P4_122$ structure at room temperature[5] and a transition at 185°C.[3]

The first studies on synthetic fischesserite by Smit, et al.[4] focused on confirming the previously-reported phase transitions by DTA and XRD.

Wiegers[6] investigated the electronic and ionic conductivity of Ag_3AuSe_2 with a claimed band gap from diffuse reflectance spectroscopy of 0.9 eV, but the samples were processed at 450°C and no evidence of their purity (XRD or otherwise) was provided. The remaining work on synthetic Ag_3AuSe_2 include a Mössbauer study showing that the ordered silver-gold chalcogenides contain monovalent Au^+ and stronger bonding than the binary chalcogenides,[7] and electromotive force measurements of thermodynamic equations of state that confirmed the stability of these compounds but did not precisely agree with the order-disorder transition temperatures.[8,9]

Ag_3AuSe_2 and Ag_3AuTe_2 are chiral and isostructural at room temperature with the space group of $I4_132$. The chirality and possible narrow band gap (or metallicity) of these materials gives rise to possible non-reciprocal and topological phenomena. In this report, we investigate the room-temperature phase of Ag_3AuSe_2.

More recently, the chirality and possible narrow band gap (or possibility of band inversion and topological phenomena) has led renewed computational focus on Ag_3AuSe_2. Faizan used density functional theory (DFT) to evaluate the promise of Ag_3AuSe_2 for thermoelectric applications, and found the band gap to be about 1.0 eV using the generalized gradient approximation (GGA).[10,11] However, published resistivity measurements (with the aforementioned question of sample purity)[6] gave a lower activation energy of around 0.5 eV. Calculations using the local density approximation (LDA), by Fang, et al. are expected to underestimate the band gap and found a gap of about 0.2 eV.[12] Bradlyn and collaborators[13] predicted it to host multifold topological crossings. Since 2016 multifold crossing in chiral topological semimetals have attracted great attention owing to their large Chern numbers,[13,14] long Fermi arcs[15–17] and optical quantized responses in terms

of Chern numbers.[18] Better understanding the band separation in Ag_3AuSe_2 is required to determine whether closing this narrow gap could lead to topological insulating behavior was examined by Sanchez-Martinez.[19] DFT-GGA calculations showed that decrease in lattice parameters result in band gap widening. In addition, they found that compression of 2% yields a meV-range band gap, which may be suitable for dark matter detector applications. All previous computational studies have pointed toward a direct band gap, but no single crystal measurements have been made, nor have diffraction data confirmed the phase purity of synthetic samples. Here, we report single crystal synthesis, transport and optical properties of Ag_3AuSe_2 and a compare computed electronic structures of the experimental and computationally-relaxed phases.

II. METHODS

Single crystals of Ag_3AuSe_2 with grains larger than 2mm were synthesized. Ag (99.9% metals basis), Au (99.98% metals basis), and Se (99.9999% metals basis) powders were mixed in a stoichiometric ratio inside an Ar filled glove box and sealed in an evacuated silica tube with 7 mm inner diameter. The ampule was placed in a muffle furnace and heated to 750°C at 1.5°C/min, annealed for 24 h, cooled to 700°C at 0.03°/min, then cooled to room temperature over 24 h. The resulting product was a solid ingot with metallic luster. A portion of the ingot was crushed and analyzed using powder X-ray diffraction (PXRD) on a Bruker D8 diffractometer with a Cu X-ray source in reflection geometry. The crystal structure was refined using the Rietveld method with GSAS-II.[20]

Ingots of Ag_3AuSe_2were manually polished with SiC grinding papers and alumina slurries down to 0.3 μm. Electron backscatter diffraction (EBSD) was performed using a Thermo Scios 2 DualBeam scanning electron microscope (SEM). We found that Ag_3AuSe_2 surface oxidizes within minutes of exposure in air, which made it difficult to obtain clear Kikuchi patterns. To avoid this issue, mechanically polished samples were milled with 7keV Ar^+ ions (Gatan PECS II) immediately before transferring into the SEM chamber. Resistivity measurements were carried out using the 2-point contact probe method in a Quantum Design PPMS DynaCool. A rod of Ag_3AuSe_2 (1.5 × 2.8 × 0.7 mm) was mounted with Kapton tape and 2 gold wire contacts were made by silver epoxy.

Spectroscopic ellipsometry measurements were performed using M-2000 and IR-VASE ellipsometers (J. A. Woollam Co.). Optical conductivity was measured in the UV-visible (0.74-6 eV) and mid-near IR (70-560 meV) energy ranges. Both ellipsometeers were calibrated with a SiO_2 (25 nm)/Si wafer prior to scanning. The experimental Ψ and Δ parameters were obtained at 70° incident angle, then converted into the real and imaginary parts

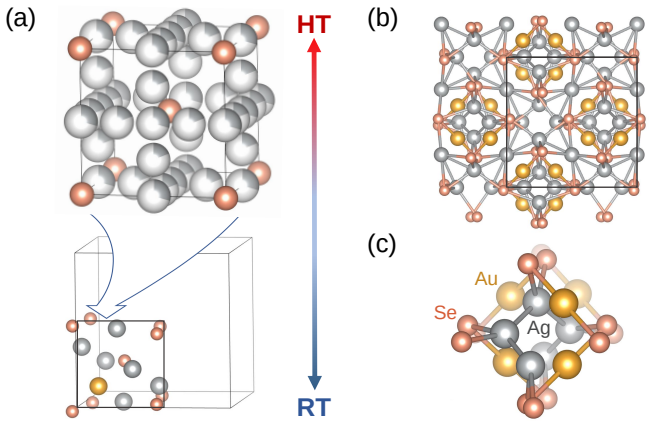


FIG. 1. The high-temperature α-Ag_2Se structure with partial Ag occupancy is shown in (a). Ag_3AuSe_2 is formed upon cooling by ordering Ag displacements and Au substitution on the α-Ag_2Se to form a unit cell that is 8 times the volume. The full unit cell of Ag_3AuSe_2 is shown in (b). (c) shows the most apparent chiral 4_1 chain viewed down <100>.

of the optical constants to satisfy the Kramers-Kronig relation. The optical conductivity determined at 60° and 80° did not change significantly, as expected for a cubic material without optical anisotropy.

First-principles density functional theory (DFT) simulations were performed using Quantum Espresso (QE)[21] and the Vienna Ab Initio Simulation Package (VASP)[22,23] with projector-augmented wave pseudopotentials. We used a variety of approximations: (1) The local density approximation (LDA), (2) the generalized gradient approximation with the Perdew-Burke-Ernzerhof parameterization (PBE),[24] (3) the modified Becke-Johnson (mBJ) method[25] and (4) the Heyd–Scuseria–Ernzerhof (HSE) approximation with the HSE06 parametrization.[26] Structural relaxations were performed with QE using PBE and a plane-wave basis with a kinetic energy cutoff of 100 Ry and a 7×7×7 k-mesh, which is stopped when pressures are below 0.1 kbar. Band calculations were performed using VASP in the presence of spin-orbit coupling, an energy cutoff of 500 eV and a 10×10×10 (5×5×5) k-mesh for LDA, PBE and mBJ (HSE06).

III. RESULTS AND DISCUSSION

A. Growth and structure

The structure of Ag_3AuSe_2 seems complex, but can be understood as a set of modification from the high-temperature α-Ag_2Se structure. Fig.1 (a) shows the body-centered-cubic $Im\bar{3}m$ α-Ag_2Se structure in which Se^{2-} ions sit at lattice points, while Ag^+ ions are statistically distributed over 4 positions on and surrounding the face centers. Upon cooling, the metal cations in

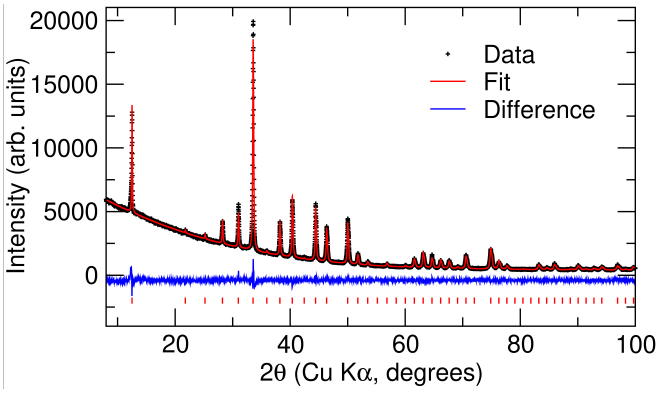


FIG. 2. Rietveld refinement to X-ray powder diffraction pattern of a crushed ingot of Ag_3AuSe_2 measured in reflection geometry.

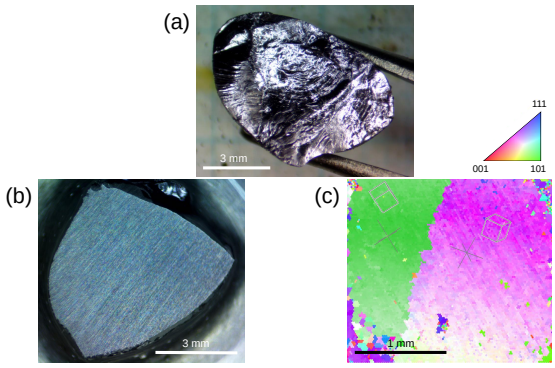


FIG. 3. Fractured and polished (1200 grit SiC) surfaces of Ag_3AuSe_2 are shown in (a) and (b), respectively. EBSD grain mapping in (c) indicates grain sizes larger than 2 mm. The green and purple regions have approximate <101> and <112> directions normal to the sample surface.

Ag_3AuSe_2 order into one of the available displaced sites, while also distributing the Au^+ evenly throughout the cell. This new distorted cell must be doubled in each direction to accommodate the Ag/Au ordering. The resulting structure of Ag_3AuSe_2 ($I4_132$ ($a = 9.96$ Å $Z = 8$) is shown in Fig. 1(b), viewed down the a axis. The chiral 4_1 ordering of the cell is best viewed down the <100> direction, forming a spiral of Ag and Au in Fig. 1(c).

Crushed ingots of Ag_3AuSe_2 gave PXRD data shown in Fig. 2, which clearly indicate phase purity and the 110 peak at $2\theta = 12.6°$ that indicates the doubled $I4_132$ ordering described in Fig. 1. As expected for a cubic material and first noted by Johan,[1] Ag_3AuSe_2 does not cleave leaving large surfaces, with a cross section of the fractured ingot shown in Fig. 3(a). The material forms large grains after cooling from the melt, so determining the grain structure from polished surfaces can be a challenge because there may be only one or few grains in cross section, such as the polished face in Fig. 3(b). Therefore, EBSD is necessary to confirm the orientation of various grains in the face. A typical cross section under EBSD mapping is shown in Fig. 3(c).

B. Electronic properties

The electrical resistivity and corresponding Arrhenius plot of Ag_3AuSe_2 are shown in Fig.4. We find that Ag_3AuSe_2 is highly resistive and exhibits a semiconductor-like temperature dependence, with an Arrhenius activation energy $E_a = 0.32$ eV, which is close to the previously reported value of 0.5 eV from Wiegers.[6] Given the different microstructures (crystal versus powder) and annealing temperatures (750 versus 450°C) between our study and that work, there may be significant differences between the defect populations that scatter carriers in the two resistivity measurements, but the activation energies are the same order of magnitude. The resistivity of Ag_3AuSe_2 is orders of magnitude greater than that of Ag_3AuTe_2 in the same structure type.[27]

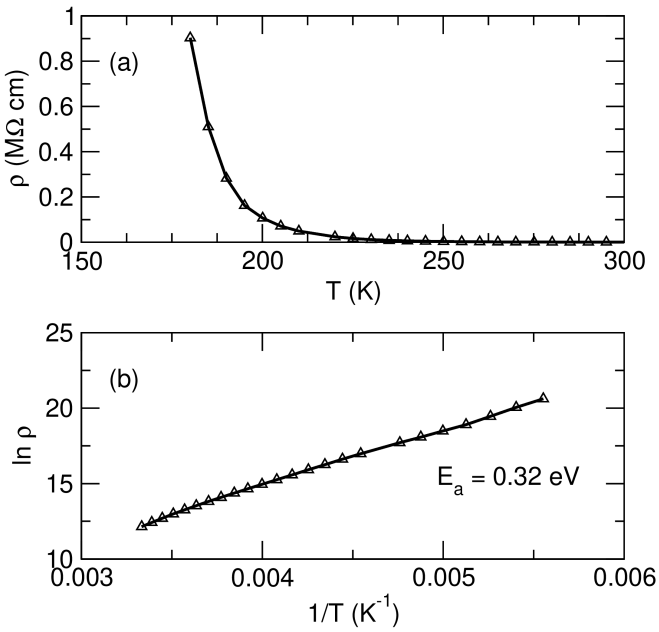


FIG. 4. Two-point electrical resistivity (a) of Ag_3AuSe_2 shows semiconducting behavior, while a linear fit to the Arrhenius plot in (b) gives an activation energy $E_a = 0.32$ eV.

In order to investigate the electronic band structure of Ag_3AuSe_2, we performed spectroscopic ellipsometry measurements. Fig. 5(a) shows the experimental optical conductivity σ_1 of Ag_3AuSe_2 measured at room temperature. No sign of free carrier response (intraband transition) was captured in the σ_1 down to the lowest frequency measured, consistent with the measured high resistivity and finite gap predicted from previous calculations.[10–12] The band gap edge of Ag_3AuSe_2 was extracted from the squared optical absorption coefficient α^2 as in Fig. 5(b). From the Fermi's golden rule and the joint density of states for parabolic bands, a frequency dependence of absorption near a direct band gap (E_G) is represented

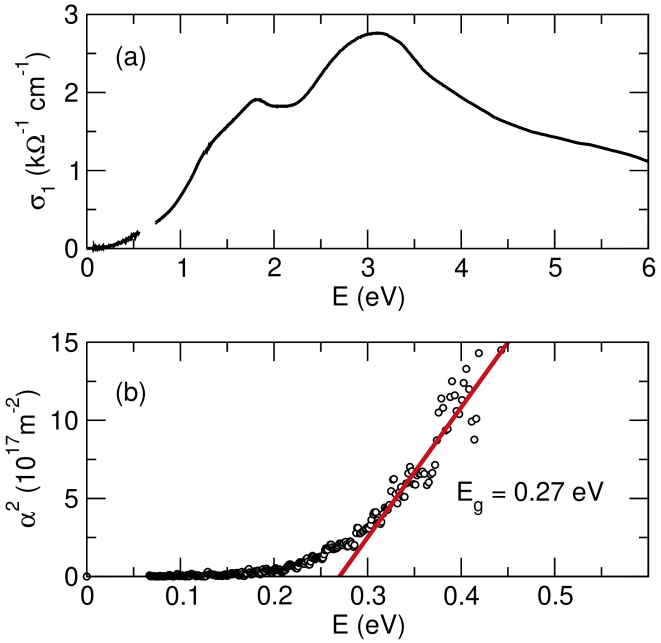


FIG. 5. Optical conductivity σ_1 (a) and the square of optical absorption coefficient α (b) for Ag_3AuSe_2 are determined by spectroscopic ellipsometry. In (b), the direct band gap edge E_g of 0.27 ($\pm$0.05) eV shown, which is estimated using the linear relation of α^2 and $(E - E_g)$ of semiconductors.[28]

as:[28]

$$\alpha \propto \sqrt{\omega - E_G}, \quad (1)$$

for $\omega > E_G$. Previous band structure studies of Ag_3AuSe_2, and our own, support parabolic curvature of the band edges of the direct gap at the Brillouin zone center Γ.[6,10,12] Using the above relation, the direct band gap of Ag_3AuSe_2 is estimated to be 0.27 eV, as illustrated in Fig. 5(b). Uncertainties in the exact onset of the rise in $alpha^2$ and the imperfect geometry of the resistivity sample measured in Fig. 4 lead to a rough agreement of both measurements to $\sim$ 0.3 eV.

Above an excitation energy of 0.27 eV the optical conductivity gradually increases and shows two clear peaks near 1.8 and 3.2 eV. These peaks arise from higher energy interband transitions, i.e. optical excitation between the valence and conduction bands that are further away from the Fermi energy. Note that there may be additional interband transitions due to the observed kink-like features in σ_1 at 1.3 eV, 4 eV and 5.5 eV.

The DFT-calculated band structures of Ag_3AuSe_2 from PBE and mBJ functionals are shown in Fig. 6. Although the gaps differ by about 1 eV, the shape and features are consistent for both functionals. A direct gap is observed at Γ and bands are symmetric around P_1. Gaps of Ag_3AuSe_2 were calculated using multiple approximations for both the experimentally-refined and DFT-PBE relaxed structures. The obtained gaps are listed in Table I. The gaps span a wide range, from fully overlapped metallic bands to 931 meV. The differences

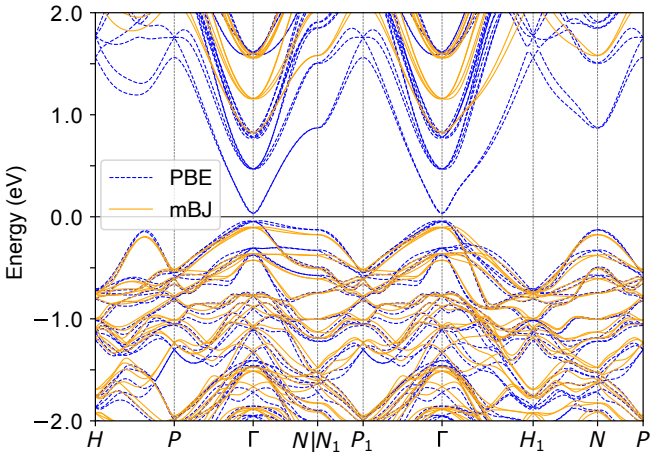


FIG. 6. DFT-calculated electronic band structures of Ag_3AuSe_2 as obtained from PBE and mBJ functionals. The general features of the band structures are equivalent for both functionals, but the direct band gap is predicted to be 71 meV for PBE and 907 meV for the hybrid mBJ functional.

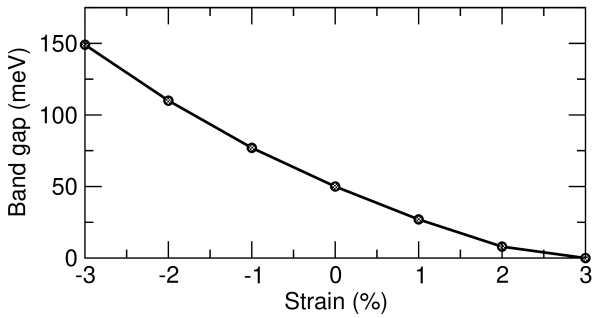


FIG. 7. The DFT-PBE band gap of the relaxed Ag_3AuSe_2 structure decreases with tensile strain, leading to band overlap around 3% strain.

between experimentally-refined and DFT-relaxed structures for a given functional are typically no larger than 30 meV, whereas the differences between LDA/PBE and the hybrid functionals mBJ/HSE06 for a given structure is much larger, over 800 meV. It is important to note that although the 30 meV differences are comparatively small, subtle differences in the atomic positions will have a large effect on transport if the band gap is of the same order of magnitude (tens of meV). These small effects are also evident in shifts of the bands due to increased overlap with compressive strain. The PBE band gaps of the Ag_3AuSe_2 DFT-PBE-relaxed structures with varying lattice strain are plotted in Fig. 7, showing an approach to metallicity as the tensile strain reaches 3%, which is a large value of strain to be reached by mechanical compression, but may be attainable by chemical substitution of the Se^{2-} anion in particular.

The noticeably larger band gap found by the hybrid mBJ and HSE functionals points to additional disorder that may lead to defect states that dominate the electronic properties of Ag_3AuSe_2. Percent-level antisite de-

	Experimental structure	DFT-PBE structure
LDA	No gap	No gap
PBE	71 meV	50 meV
mBJ	931 meV	928 meV
HSE06	907 meV	872 meV

TABLE I. DFT-calculated band gaps of Ag_3AuSe_2 for experimentally-refined structures and DFT-PBE-relaxed structures. Four pairs of ab-initio calculations using the LDA, PBE, mBJ and HSE06 approximations for the exchange correlation energy are used.

fects in the Ag/Au ordering that occurs at the 270°C order-disorder transition would be challenging to quantify, and would likely remain coherent with the large-grained microstructure. Additional single-crystal diffraction may shed light on this possibility. Additionally, more detailed investigation of the optical properties, including angle-resolved photoemission spectroscopy, should correlate larger features of the conduction band with first-principles results, rather than states exclusively near band edges. Understanding these details for the entire class of fischesserite-type phases will reveal their potential for nonlinear optics and topological responses.

IV. CONCLUSIONS

We have established that large single crystals of Ag_3AuSe_2 can be grown by slow-cooling from the melt. Ellipsometry and resistivity measurements point to an activation energy and optical band gap around 0.3 eV, which is between the PBE-estimated band gap of 0.07 eV (which should be an underestimation) and the mBJ and HSE06 band gaps of about 0.9 eV, which we expect to be accurately predicted. Given the sensitivity of the band gap to strain, and the necessary order-disorder transition that Ag_3AuSe_2 experiences on cooling, it follows that subtle tuning of the defect population, surface treatment, and stoichiometry of Ag_3AuSe_2 and the related fischesserite-petzite family of materials can lead to intentional tuning of the band gap. It remains to be seen whether a band inversion can be obtained upon application of pressure of chemical substitution with the telluride.

V. ACKNOWLEDGMENTS

This study was supported by the Center for Quantum Sensing and Quantum Materials, an Energy Frontier Research Center funded by the U. S. Department of Energy, Office of Science, Basic Energy Sciences under Award DE-SC0021238. The authors acknowledge the use of facilities and instrumentation at the Materials Research Laboratory Central Research Facilities, University of Illinois, partially supported by NSF through the University of Illinois Materials Research Science and Engineering Center DMR-1720633. MGV, IE and MGA acknowledge the Spanish Ministerio de Ciencia e Innovación (grant number PID2019109905GB-C21) and Programa Red Guipuzcoana de Ciencia, Tecnología e Innovación 2021 No. 2021-CIEN-000070-01 Gipuzkoa Next. MGV thanks support from the DeutscheForschungsgemeinschaft (DFG, German Research Foundation) GA 3314/1-1 – FOR5249 (QUAST). SB acknowledges support through the Early Postdoc Mobility Fellowship from the Swiss National Science Foundation (Grant number P2EZP2 191885). BL, JSS, and TWN were supported by the Institute for Basic Science (IBS) in Korea (Grant No. IBS-R009-D1).

* dpshoema@illinois.edu

[1] Z. Johan, P. Picot, R. Pierrot, and M. Kvacek, Bull. Soc. Fr. Mineral. Crist. **94**, 381 (1971).
[2] L. Bindi and C. Cipriani, Canad. Mineral. **42**, 1733 (2004).
[3] B. H. Tavernier, J. Vervecken, P. Messien, and M. Baiwir, Z. Anorg. Allg. Chem. **356**, 77 (1967).
[4] T. J. M. Smit, E. Venema, J. Wiersma, and G. A. Wiegers, J. Solid State Chem. **2**, 309 (1970).
[5] M. D. Barton, C. Kieft, E. A. J. Burke, and I. S. Oen, Canad. Mineral. **16**, 651 (1978).
[6] G. A. Wiegers, J. Less Common Met. **48**, 269 (1976).
[7] F. E. Wagner, J. A. Sawicki, J. Friedl, J. A. Mandarino, and D. C. Harris, Canad. Mineral. **30**, 327 (1992).
[8] E. G. Osadchii and E. A. Echmaeva, **92**, 640, publisher: De Gruyter.
[9] D. Feng and P. Taskinen, J. Alloys Compd. **583**, 176 (2014).
[10] M. Faizan, G. Murtaza, S. Azam, S. A. Khan, A. Mahmood, and A. Yar, Mater. Sci. Semicon. Proc. **52**, 8 (2016).
[11] M. Faizan, H. Ullah, S. H. Khan, S. M. Ramay, S. A. S. Qaid, A. Mahmood, and M. Ali, Int. J. Mod. Phys. B **31**, 1750253 (2017).
[12] C. Fang, R. Groot, and G. Wiegers, J. Phys. Chem. Solids **63**, 457 (2002).
[13] B. Bradlyn, J. Cano, Z. Wang, M. Vergniory, C. Felser, R. J. Cava, and B. A. Bernevig, Science **353** (2016).
[14] G. Chang, S.-Y. Xu, B. J. Wieder, D. S. Sanchez, S.-M. Huang, I. Belopolski, T.-R. Chang, S. Zhang, A. Bansil, H. Lin, and M. Z. Hasan, Phys. Rev. Lett. **119**, 206401 (2017).
[15] N. B. Schröter, D. Pei, M. G. Vergniory, Y. Sun, K. Manna, F. De Juan, J. A. Krieger, V. Süss, M. Schmidt, P. Dudin, *et al.*, Nature Physics **15**, 759 (2019).
[16] N. B. Schröter, S. Stolz, K. Manna, F. De Juan, M. G. Vergniory, J. A. Krieger, D. Pei, T. Schmitt, P. Dudin, T. K. Kim, *et al.*, Science **369**, 179 (2020).
[17] D. S. Sanchez, I. Belopolski, T. A. Cochran, X. Xu, J.-X. Yin, G. Chang, W. Xie, K. Manna, V. Süß, C.-Y. Huang, N. Alidoust, D. Multer, S. S. Zhang, N. Shumiya, X. Wang,

G.-Q. Wang, T.-R. Chang, C. Felser, S.-Y. Xu, S. Jia, H. Lin, and M. Z. Hasan, Nature **567**, 500 (2019).
[18] F. Flicker, F. De Juan, B. Bradlyn, T. Morimoto, M. G. Vergniory, and A. G. Grushin, Physical Review B **98**, 155145 (2018).
[19] I. Sánchez-Martínez, M.-Áand Robredo, A. Bidaurrazaga, A. Bergara, F. d. Juan, A. G. Grushin, and M. G. Vergniory, J. Phys.: Mater. **3**, 014001 (2019).
[20] B. H. Toby and R. B. Von Dreele, J. Appl. Cryst. **46**, 544 (2013).
[21] P. Giannozzi, O. Andreussi, T. Brumme, O. Bunau, M. B. Nardelli, M. Calandra, R. Car, C. Cavazzoni, D. Ceresoli, M. Cococcioni, N. Colonna, I. Carnimeo, A. D. Corso, S. de Gironcoli, P. Delugas, R. A. D. Jr, A. Ferretti, A. Floris, G. Fratesi, G. Fugallo, R. Gebauer, U. Gerstmann, F. Giustino, T. Gorni, J. Jia, M. Kawamura, H.-Y. Ko, A. Kokalj, E. Küçükbenli, M. Lazzeri, M. Marsili, N. Marzari, F. Mauri, N. L. Nguyen, H.-V. Nguyen, A. O. de-la Roza, L. Paulatto, S. Poncé, D. Rocca, R. Sabatini, B. Santra, M. Schlipf, A. P. Seitsonen, A. Smogunov, I. Timrov, T. Thonhauser, P. Umari, N. Vast, X. Wu, and S. Baroni, J. Phys. Cond. Mat. **29**, 465901 (2017).
[22] G. Kresse and J. Furthmüller, Phys. Rev. B **54**, 11169 (1996).
[23] G. Kresse and J. Furthmüller, Comput. Mater. Sci. **6**, 15 (1996).
[24] J. P. Perdew, K. Burke, and M. Ernzerhof, Phys. Rev. Lett. **77**, 3865 (1996).
[25] F. Tran and P. Blaha, Phys. Rev. Lett. **102**, 226401 (2009).
[26] J. Heyd, G. E. Scuseria, and M. Ernzerhof, J. Chem. Phys. **118**, 8207 (2003).
[27] D. P. Young, C. L. Brown, P. Khalifah, R. J. Cava, and A. P. Ramirez, J. Applied Phys. **88**, 5221 (2000).
[28] A. Fox and D. Fox, *Optical Properties of Solids* (Oxford University Press, 2001).